ZnCdSe/ZnCdMgSe quantum cascade electroluminescence

Kale J. Franz,[1,a)] William O. Charles,[2] Aidong Shen,[2] Anthony J. Hoffman,[1] Maria C. Tamargo,[3] and Claire Gmachl[1]
[1]*Department of Electrical Engineering, Princeton University, Princeton, New Jersey 08544, USA*
[2]*Department of Electrical Engineering, The City College of New York, New York, New York 10031, USA*
[3]*Department of Chemistry, The City College of New York, New York, New York 10031, USA*

(Received 21 January 2008; accepted 6 March 2008; published online 25 March 2008)

This letter reports electroluminescence emission from a ZnCdSe/ZnCdMgSe quantum cascade (QC) structure. With a two-well QC active region design, the II-VI heterostructure was grown lattice matched on an InP substrate by molecular beam epitaxy. Deep etched mesas were electrically pumped at current densities up to 10 kA/cm^2, producing optical emission centered near 4.8 μm, in good agreement with the structure design. The light is predominantly TM polarized, confirming its intersubband origin. Electroluminescence was observed from 78 to 300 K. © *2008 American Institute of Physics*. [DOI: 10.1063/1.2903135]

Quantum cascade (QC) development has enabled robust generation of mid-infrared light. To date, the workhorse material for mid-infrared QC lasers has been the InGaAs/AlInAs material system;[1] lasers from this material have reached the technological benchmark of room temperature, continuous wave operation.[2] However, performance is not as advanced at wavelengths below 4 μm. Such high energy photon generation in QC structures is fundamentally limited by the band offset between the well and barrier materials in the relevant carrier transport band. In addressing this fundamental limit, Sb-based III-V heterostructures have demonstrated the shortest wavelength operation to date achieved for any QC laser: 2.75 μm.[3] Sb-based materials are appealing for short-wavelength QC lasers because of their large Γ valley conduction band offsets—in InAs/AlSb up to 2.1 eV.[4] In this material system, however, scattering out of the upper laser energy state into satellite valleys limits the "effective" usable band offset to ~0.75 eV.[4]

Materials systems other than III-V antimonides have been proposed to address the challenges of shorter-wavelength photon generation through intersubband transitions. GaN/AlGaN QC structures have shown intersubband photoluminescence at $\lambda \approx 2.13$ μm[5] and GaN/AlGaN QC photodetectors have been demonstrated with responsitivity near $\lambda \approx 1.7$ μm.[6] Electroluminescence from CdF_2/CaF_2 QC structures grown on Si has also been reported.[7]

We have previously proposed the $Zn_{0.43}Cd_{0.47}Se/Zn_{0.09}Mg_{0.91}Se$ system grown lattice matched on InP as a large band offset QC emitter alternative.[8,9] The ZnCdSe/ZnMgSe system has a Γ valley band offset of 1.2 eV (Ref. 8); all of it is usable for QC laser design due to the absence of satellite valleys.[10] Such design space makes ZnCdSe/ZnMgSe QC emitters possible near 1.5 μm. Alternately, because of magnesium's susceptibility to oxidation, the $Zn_{0.43}Cd_{0.57}Se/Zn_{0.20}Cd_{0.19}Mg_{0.61}Se$ variant is currently more technologically practicable.[9] Here, we demonstrate initial steps toward a II-VI QC laser, with the development of a ZnCdSe/ZnCdMgSe QC structure that exhibits intersubband electroluminescence (EL).

We have developed a conventional two-well active region QC structure in the $Zn_{0.43}Cd_{0.57}Se/Zn_{0.20}Cd_{0.19}Mg_{0.61}Se$ material system. The Fig. 1 conduction band diagram shows the structure for an applied field of 67 kV/cm; a single stage of the layer sequence is (in angstroms starting from the injection barrier ***I***, and going from left to right in the direction of electron flow) **30**/34/**10**/28/**20**/24/**10**/22/**12**/20/**16**/20/**18**/18/**18**/18/**20**/16/**20**/16/**20**/14/**22**/14/**24**/12/**26**/12. ZnCdMgSe barriers are in boldface and ZnCdSe wells are in normal font. Underlined layers represent ZnCdSe that is Cl doped (2×10^{17} cm^{-3}) and ZnCdMgSe doped with the same $ZnCl_2$ flux as the ZnCdSe layers. We estimate a sheet density per active region-injector period of $n_{2D}=5.4\times10^{11}$ cm^{-2}. We designed an optical transition of 284 meV (4.37 μm) with a calculated optical dipole matrix element $z_{32}=8.7$ Å. An active region energy state is placed 32 meV below the lower optical transition level, sufficient for longitudinal optical phonon depopulation of the lower laser state via ZnSe-like (31.6 meV) (Ref. 11) and CdSe-like (26.3 meV) (Ref. 12) phonons. This configuration results in a calculated upper state lifetime $\tau_3=0.84$ ps, lower state lifetime $\tau_2=0.21$ ps, and nonradiative transition time $\tau_{32}=3.3$ ps. We considered

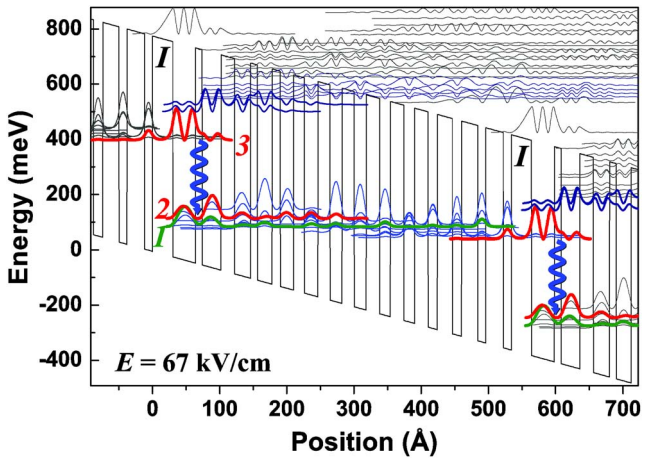

FIG. 1. (Color online) A portion of the conduction band energy diagram under an applied field of 67 kV/cm. $Zn_{0.43}Cd_{0.57}Se$ wells and $Zn_{0.20}Cd_{0.19}Mg_{0.61}Se$ barriers are used to create a 284 meV optical transition, represented by wavy arrows. The injection barrier is signified by ***I***.

a)Electronic mail: kfranz@princeton.edu.

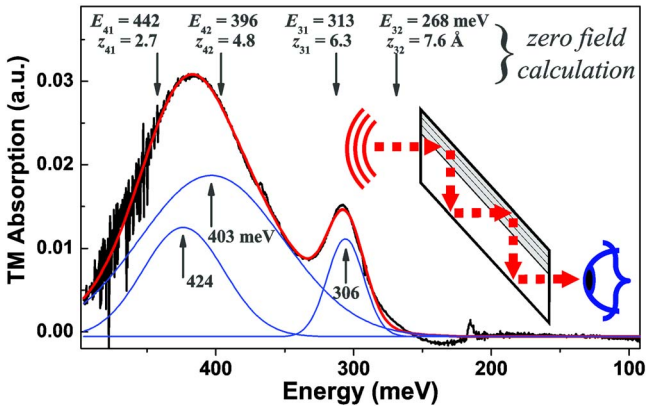

FIG. 2. (Color online) Transverse magnetic absorption spectrum from multipass transmission analysis. Fitted Gaussians show three resolvable peaks. Optical transition calculations for zero applied field are indicated at the top. The inset shows the multipass configuration with broadband light passing through a sample polished to 45° on both ends.

band gaps of 2.08 and 3.03 eV for $Zn_{0.43}Cd_{0.57}Se$ and $Zn_{0.20}Cd_{0.19}Mg_{0.61}Se$, respectively, with a conduction band offset of 0.78 eV (Ref. 13). The corresponding conduction band effective masses are calculated to be 0.128 and 0.181 times the free electron mass (Ref. 13), respectively.

The QC emitter was grown by molecular beam epitaxy on a low doped ($n < 2\times10^{17}$ cm^{-3}) InP:S substrate.[14] Prior to active core growth, we deposited 0.25 μm of $In_{0.53}Ga_{0.47}As$ (Si doped 5×10^{17} cm^{-3}) as buffer layer. II-VI growth was preceded by a 40 s Zn flux treatment and 100 Å of low temperature (230 °C) ZnCdSe (Cl doped 2×10^{17} cm^{-3}). At the 330 °C growth temperature, another 400 Å of ZnCdSe (Cl doped 2×10^{17} cm^{-3}) buffer was deposited. Ten periods of the active region-injector sequence were grown. The structure was capped by 400 Å ZnCdSe (Cl doped 2×10^{17} cm^{-3}) and 2000 Å ZnCdSe (Cl doped 4×10^{18} cm^{-3}). Digital transition gradings were used between bulk layers and the active core.

Polarization-dependent multipass transmission measurements were performed using a Fourier transform infrared (FTIR) spectrometer on a sample with each end polished to 45°. Two dominant transverse magnetic (TM) absorption peaks were observed, shown in Fig. 2, within which we were able to fit three Gaussian curves. Calculations for zero field energy transitions are indicated in Fig. 2 and are consistent with the observed absorption.

EL structures were fabricated in the form of semicircular cleaved mesas. Lithographically patterned 400 μm diameter circles were etched into mesa structures using a $HBr:HNO_3:H_2O$ (1:1:10) wet chemical etch solution; the etch depth was sufficient to penetrate the epitaxially grown material. A second lithography step was used to apply the top contact metallization. An O_2 plasma cleaning followed by a 45 s $HF:H_2O$ (1:1) dip immediately preceded top metal contact deposition. Top contacts consisted of 150 Å Ti followed by 2500 Å Au; Ge/Au back-side InP contacts were also deposited. Finally, the mesas were cleaved into semicircular EL structures and In soldered to Cu heat sinks; the top electrical contacts were wire bonded to contact pads. Cleaved mesa areas were measured as around 0.036 mm^2.

EL was collected for a variety of heat sink temperatures and applied current values using an FTIR spectrometer in step scan mode and a cooled HgCdTe detector. The applied current pulses were 1 μs in duration at 3% duty cycle.

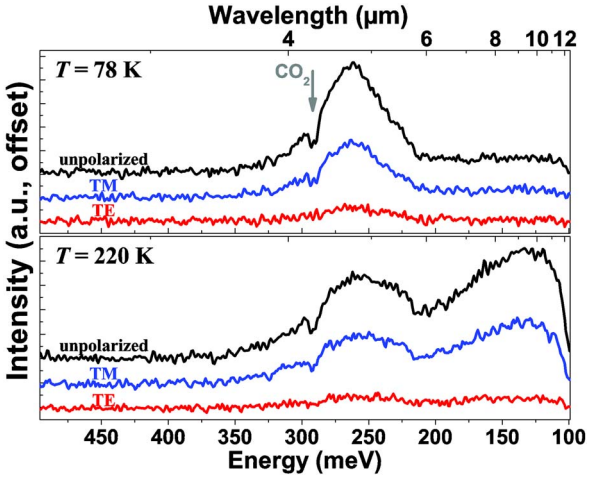

FIG. 3. (Color online) Polarization-resolved EL spectra for a device driven with 9.6 kA/cm^2 at 78 K (top) and 220 K (bottom). The emission is predominantly TM polarized. Additional longer wavelength light is seen at higher heat sink temperatures and currents. Atmospheric CO_2 absorption can be seen near $\lambda \approx 4.2$ μm. Spectra are not corrected for detector responsivity, which is more sensitive at longer wavelengths.

We observed EL centered near $\lambda \approx 4.8$ μm. Emission polarization characteristics were examined to confirm intersubband light generation; intersubband optical transitions in quantum wells are TM polarized. Two exemplary results of polarization-resolved EL spectra are shown in Fig. 3 for heat sink temperatures of 78 and 220 K and a pumping current of 9.6 kA/cm^2. While a small amount of transverse electric light is observed, which we attribute to scattering from within the rounded mesa, the EL is predominantly TM polarized.

At low temperatures, the primary emission peak is observed near 4.8 μm. Figure 4 shows emission behavior with increasing current for a heat sink temperature of 78 K and no polarizer in the optical path. The 4.8 μm emission peak correspondingly grows with increasing pumping current. At a pumping current density of 2.8 kA/cm^2, a Gaussian fit gives the EL full width at half-maximum (FWHM) as 52 meV; at 9.6 kA/cm^2, the FWHM is 47 meV, which is about 20% of the transition energy.

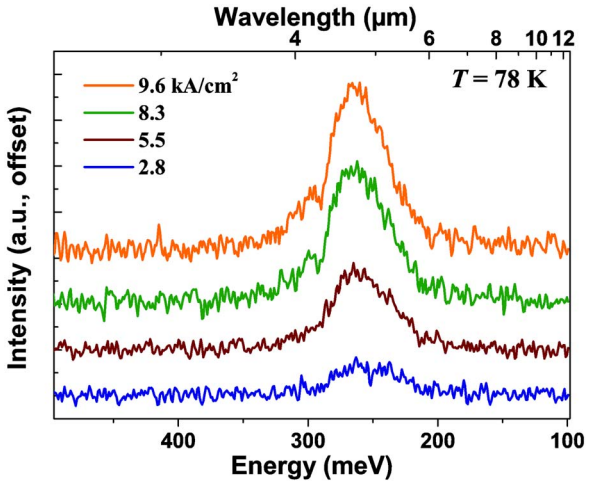

FIG. 4. (Color online) EL spectra at T=78 K and various current levels as indicated. Emission is centered near 4.8 μm.

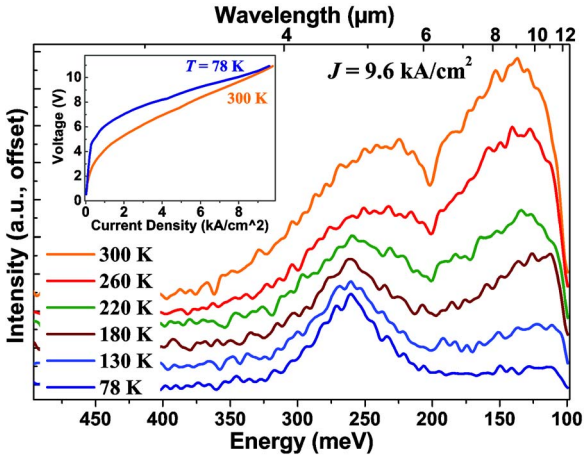

FIG. 5. (Color online) EL spectra at 9.6 kA/cm^2 for heat sink temperatures from 78 to 300 K. Additional longer-wavelength light is seen with increasing temperature. Over the 78–300 K temperature range, the ~4.8 μm peak intensity decreases by 30% and emission width increases by 36%. Spectra are not corrected for variations in detector responsivity, which are more sensitive at longer wavelengths. The inset shows current-voltage curves at 78 and 300 K.

This 4.8 μm light is seen at temperatures ranging from 78 to 300 K. Figure 5 shows spectra with increasing temperature for a pumping current density of 9.6 kA/cm^2. All spectra represent TM polarized light with subtraction of the corresponding unpolarized background. The emission peak centered near 4.8 μm is present over the full temperature range. We also observed the growth of a secondary, temperature-induced, lower energy emission. This broad emission is more intense for both higher currents and higher temperatures. Reported spectra are not corrected for wavelength-dependent variations in detector responsivity; we estimate that our detector is 55% more sensitive for 120 meV photons than for 260 meV photons. While the origin of this low energy emission is still under investigation, the 4.8 μm intersubband emission is dominant and persists through room temperature. This intersubband emission has the well-known temperature-dependent behavior: from 78 to 300 K, Gaussian fits that include a rising background show that peak intensity decreases by 30% and emission width increases by 36%.

The current-voltage curves in the inset of Fig. 5 show typical QC behavior, with characteristic current turn on once sufficient voltage has been applied. The turn on for 78 K occurs at 5.40 V. At a turn-on field of 64 kV/cm, 3.42 V is dropped over the active core. We attribute to conduction band offsets at bulk interfaces another 0.35 V. The remaining 1.63 V is likely dropped over the as yet nonideal top contacts.

In conclusion, we have designed, grown, and tested a ZnCdSe/ZnCdMgSe QC structure exhibiting room temperature EL. The II-VI intersubband emitter has primarily TM polarized emission centered near 4.8 μm in good agreement with the as-designed structure.

This work is supported in part by MIRTHE (NSF-ERC No. EEC-0540832), NASA URC COSI Grant No. NCC-1-03009, and Department of Defense Grant No. W911NF-04-01-0023. K.J.F. gratefully acknowledges the support of the National Science Foundation Graduate Research Fellowship Program.

[1] C. Gmachl, F. Capasso, D. L. Sivco, and A. Y. Cho, Rep. Prog. Phys. **64**, 1533 (2001).
[2] M. Beck, D. Hofstetter, T. Aellen, J. Faist, U. Oesterle, M. Ilegems, E. Gini, and H. Melchior, Science **295**, 301 (2002); L. Diehl, D. Bour, S. Corzine, J. Zhu, G. Hofler, M. Loncar, M. Troccoli, and F. Capasso, Appl. Phys. Lett. **88**, 201115 (2006).
[3] J. Devenson, O. Cathabard, R. Teissier, and A. N. Baranov, Appl. Phys. Lett. **91**, 251102 (2007).
[4] J. Devenson, R. Teissier, O. Cathabard, and A. N. Baranova, Appl. Phys. Lett. **90**, 111118 (2007).
[5] L. Nevou, M. Tchernycheva, F. H. Julien, F. Guillot, and E. Monroy, Appl. Phys. Lett. **90**, 121106 (2007).
[6] A. Vardi, G. Bahir, F. Guillot, C. Bougerol, E. Monroy, S. E. Schacham, M. Tchernycheva, and F. H. Julien, Appl. Phys. Lett. **92**, 011112 (2008).
[7] K. Jinen, T. Kikuchi, M. Watanabe, and M. Asada, Jpn. J. Appl. Phys., Part 1 **45**, 3656 (2006).
[8] M. Sohel, M. Munoz, and M. C. Tamargo, Appl. Phys. Lett. **85**, 2794 (2004).
[9] H. Lu, A. Shen, M. C. Tamargo, C. Y. Song, H. C. Liu, S. K. Zhang, R. R. Alfano, and M. Munoz, Appl. Phys. Lett. **89**, 131903 (2006).
[10] M. C. Tamargo, *II-VI Semiconductor Materials and their Applications* (CRC, New York, 2002).
[11] D. Walsh, K. Mazuruk, and M. Benzaquen, Phys. Rev. B **36**, 2883 (1987).
[12] P. Y. Yu, Solid State Commun. **19**, 1087 (1976).
[13] M. Munoz, H. Lu, X. Zhou, M. C. Tamargo, and F. H. Pollak, Appl. Phys. Lett. **83**, 1995 (2003).
[14] W. O. Charles, A. Shen, K. J. Franz, C. Gmachl, Q. Zhang, Y. Gong, G. F. Neumark, and M. C. Tamargo, Proceedings of the North American Conference on Molecular Beam Epitaxy, 2007 (unpublished).